


Article

Interference Effects in Fully Differential Ionization Cross Sections near the Velocity Matching in P + He Collisions

Sujan Bastola ¹, Madhav Dhital ^{1,2}, Shruti Majumdar ¹, Ahmad Hasan ³, Ramaz Lomsadze ⁴, Jacob Davis ¹, Basu Lamichhane ^{1,5}, Sandor Borbély ⁶ , Ladislau Nagy ⁶ and Michael Schulz ^{1,*}

¹ Physics Department and LAMOR, Missouri University of Science & Technology, Rolla, MO 65409, USA

² Physics Department, University of California-Riverside, Riverside, CA 92521, USA

³ Department of Physics, UAE University, Abu Dhabi P.O. Box 15551, United Arab Emirates

⁴ Department of Exact and Natural Science, Tbilisi State University, Tbilisi 0179, Georgia

⁵ Natural Sciences Collegium, Eckerd College, St. Petersburg, FL 33711, USA

⁶ Faculty of Physics, Babeş-Bolyai University, 400084 Cluj, Romania

* Correspondence: schulz@mst.edu

Abstract: We performed a fully differential experimental and theoretical study on ionization of He in intermediate-energy collisions with protons for a small projectile coherence length. Data were taken for an ejected electron energy corresponding to a speed close to the projectile speed (velocity matching). In the fully differential angular electron distributions, a pronounced double-peak structure, observed previously for a coherence length much larger than the atomic size, is much less pronounced in the current data. This observation is interpreted in terms of interference between first- and higher-order transition amplitudes. Although there is large quantitative disagreement between experiment and theory, the qualitative agreement supports this interpretation.

Keywords: atomic collisions; ionization; coherence



Citation: Bastola, S.; Dhital, M.; Majumdar, S.; Hasan, A.; Lomsadze, R.; Davis, J.; Lamichhane, B.; Borbély, S.; Nagy, L.; Schulz, M. Interference Effects in Fully Differential Ionization Cross Sections near the Velocity Matching in P + He Collisions. *Atoms* **2022**, *10*, 119. <https://doi.org/10.3390/atoms10040119>

Academic Editor: Emmanouil P. Benis

Received: 19 September 2022

Accepted: 17 October 2022

Published: 24 October 2022

Publisher's Note: MDPI stays neutral with regard to jurisdictional claims in published maps and institutional affiliations.



Copyright: © 2022 by the authors. Licensee MDPI, Basel, Switzerland. This article is an open access article distributed under the terms and conditions of the Creative Commons Attribution (CC BY) license (<https://creativecommons.org/licenses/by/4.0/>).

1. Introduction

One of the major motivations for atomic collision research is to gain insight into the fundamentally important few-body problem (FBP) [1,2]. The FBP has its roots in the Schrödinger equation not being solvable in closed form for more than two mutually interacting particles, even when the forces acting within and on the system are known with high accuracy. Theoretically, the FBP in atomic collisions has been tackled by perturbative [2–10] and, more recently, by non-perturbative [1,11–15] approaches. In treatments employing the Born series, understanding the few-body dynamics of the collision basically means precisely calculating the relative contributions of the leading-order process to the various higher-order processes to the cross sections. In contrast, in distorted wave and non-perturbative methods, these contributions usually do not occur as separate terms in the transition amplitude (as they do in the Born series). There, the accuracy of the description of higher-order processes depends on how well the exact final-state wavefunction of the collision system is approximated (distorted wave methods) or on the size of the basis set and on the appropriate selection of the basis states (non-perturbative methods).

Here, our interest is focused on ionization of the target by ion impact. There, one higher-order process that has been investigated by many groups is referred to as post-collision interaction (PCI) [16–25]. PCI involves at least two interactions between the projectile and the active target electron. In the primary encounter, the electron absorbs sufficient energy from the projectile to be ejected into the continuum. In the subsequent interaction, the ejected electron and the projectile are focused toward the initial beam axis in the outgoing part of the collision. In order to conserve momentum, the residual target ion needs to be involved as well, i.e., momentum exchange must occur between the recoil ion and the electron or the projectile [22]. PCI is particularly prominent for electrons ejected

with an energy corresponding to a speed close to the projectile speed (velocity matching). Pronounced signatures of PCI have been observed in ejected electron spectra [16,17,19,21], in residual target-ion spectra [20], and in scattered projectile spectra [18,22,25].

The most sensitive data on the reaction dynamics in atomic collisions are offered by fully differential cross sections (FDCS) measured in kinematically complete experiments (for reviews, see [26–28]). If the first-order mechanism is the dominant contribution to the FDCS, the angular-ejected electron distribution exhibits a characteristic double-peak structure, with the binary peak occurring in the direction of the momentum transfer \mathbf{q} and the recoil peak in the direction of $-\mathbf{q}$ [2,29]. However, for low-energy ions and/or ions with large charge state, these structures are shifted in the forward direction relative to \mathbf{q} or $-\mathbf{q}$, respectively, due to PCI [30–34] (often, the recoil peak disappears altogether). If the ejected electron energy corresponds to the velocity matching region, another signature of PCI is observed: it then leads to a pronounced peak structure occurring in the initial projectile beam direction (forward peak), which at large scattering angles θ_p is separated from the binary peak by a minimum [23,35,36]. The forward peak can be understood in terms of a mutual focusing effect between the projectile and the ejected electron in the outgoing part of the collision. For electron impact such a focusing does not occur because of the repulsive nature of the underlying force. Therefore, the forward peak can only be studied in collisions of ions or positrons with atoms or molecules.

At first glance, separate forward and binary peak structures may appear plausible, at least if the binary peak is basically viewed as being due to the first-order process and the forward peak as being due to PCI. Because of momentum conservation, the binary peak is then expected near the direction of \mathbf{q} and the forward peak, due to the focusing effect caused by PCI, at 0° . However, as stated in the previous paragraph, the binary peak cannot entirely be attributed to the first-order process, but rather, the forward shift is a signature of PCI as well. The presence of the forward peak and the shift of the binary peak are then just two different manifestations of the same mechanism, which only differ quantitatively in the shift relative to \mathbf{q} . This raises the question of why a relatively small shift (binary peak) and a large shift (forward peak) are very likely, but an intermediate shift (minimum separating both peaks) is less likely. Classically, one would expect a single peak with a centroid somewhere between the direction of \mathbf{q} and 0° with a wing on the small-angle side extending toward 0° . On the other hand, in quantum mechanics, a possible explanation for the double-peak structure is based on interference between the first-order and higher-order amplitudes.

For interference to be observable experimentally, the incoming projectile must be coherent [37,38]. The importance of such projectile coherence effects has been confirmed by theory [39–41]. The transverse coherence length Δx can be manipulated, such as in classical optics, in terms of a collimating slit placed before the target [37,38]. The geometry of the collimating slit affects the experimental resolution, but it can also have an impact on the quantum mechanical position uncertainty, i.e., the coherence length of the incoming projectile wave. For example, for a narrow slit placed at a large distance from the target, the local collimation angle that the slit subtends relative to the target corresponds to a sharp transverse projectile momentum distribution. According to the Heisenberg uncertainty relation, this corresponds to a large dimension over which the projectile can coherently illuminate the target, i.e., to a large transverse coherence length Δx . Likewise, a broad slit placed at a small distance from the target corresponds to a small Δx .

Increasing the width of the collimating slit has a direct negative impact on the experimental resolution. However, changing the slit distance does not affect the resolution significantly. The reason is that if one wants to measure cross sections as a function of the projectile scattering angle, it is necessary to place the focus of the projectile beam as far beyond the target as possible. In the ideal scenario, where the focal point approaches an infinite distance from the target, the angular spread of the beam approaches zero, regardless of the slit distance. Therefore, by changing the slit distance, one can manipulate the coherence length without compromising the experimental resolution. Our previous studies, reporting

a double forward/binary peak structure [35,36], were performed for a relatively large slit distance, corresponding to Δx larger than 3 a.u. Here, we report on a measurement with $\Delta x < 1$ a.u. under otherwise identical conditions. The double-peak structure is found to be much less pronounced, if present at all, for the smaller coherence length. This supports the interpretation that the double-peak structure is caused by interference between the first- and higher-order transition amplitudes. This finding is qualitatively also backed by our calculations.

2. Experiment

The experiment was performed at the medium-energy accelerator of the Missouri University of Science and Technology. A schematic sketch of the set-up is shown in Figure 1. A proton beam with an energy spread of much less than 1 eV was generated with a hot-cathode ion source and accelerated to an energy of 75 keV using a high-voltage platform. The beam was collimated by a pair of slits with a width of 150 μm before entering the target chamber. The vertical slit (collimation in x-direction) was placed at a distance of 7 cm from the target and the horizontal slit (collimation in y-direction) at a distance of 50 cm. The slit geometry for the horizontal slit corresponds to a transverse coherence length Δy of more than 3 a.u. The collimating slit can only increase, but not decrease the coherence length compared to an uncollimated beam. In the x-direction, the vertical slit would lead to a transverse coherence length of 0.5 a.u. if the uncollimated beam was completely incoherent. However, because of apertures in the accelerator terminal, the actual transverse coherence length in the x-direction is $\Delta x \approx 1$ a.u. In the longitudinal direction, the coherence length is determined by the intrinsic energy spread of the projectiles. Since the intrinsic energy spread cannot be larger than the total energy spread, corresponding to a momentum uncertainty of 0.02 a.u., the latter provides a lower limit for the longitudinal coherence Δz of about 50 a.u. Therefore, the beam can be regarded as longitudinally coherent.

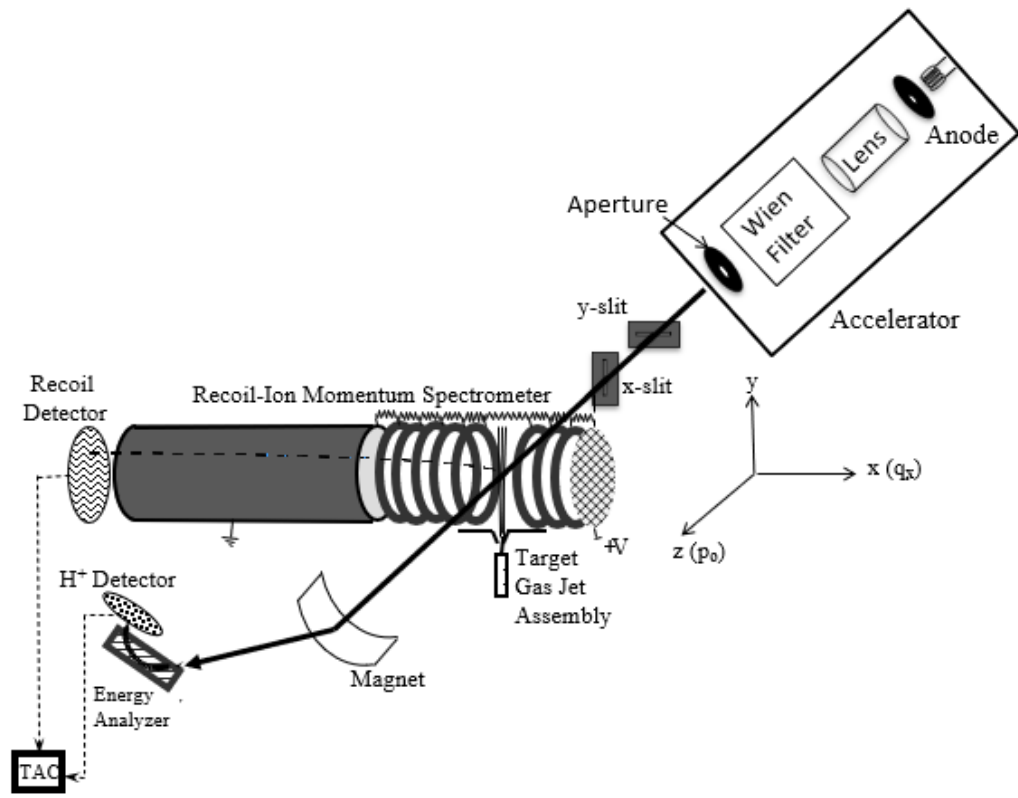


Figure 1. Schematic sketch of the experimental set-up.

In the target chamber, the projectile beam was crossed with a very cold ($T \approx 1\text{--}2$ K) atomic He beam from a supersonic gas jet propagating in the vertical direction. The

scattered protons that did not charge exchange were selected with a switching magnet and decelerated to an energy of 5 keV using another high-voltage platform. The projectiles were then energy analyzed with an electrostatic parallel-plate analyzer [42] and detected with a two-dimensional position sensitive micro-channel plate detector (MCP). The entrance and exit slits of the analyzer had a length of several cm in the horizontal (x-direction) and a width of 75 μm in the vertical direction (y-direction). The analyzer was set to a pass energy corresponding to an energy loss of $\epsilon = 68.5$ eV with a resolution of 2.5 eV full width at half maximum (FWHM). From ϵ the longitudinal component and from the position the x-component of the scattered projectile momentum were determined. Due to the narrow width of the slits, the y-component was fixed at 0, and the projectile transverse coherence properties were primarily determined by Δx . The momentum transfer is defined by $\mathbf{q} = \mathbf{p}_o - \mathbf{p}_f$, where \mathbf{p}_o and \mathbf{p}_f are the initial and final projectile momenta, and θ_p was determined by $\tan \theta_p = q_x/p_o$. The resolution in θ_p was 0.12 mrad FWHM.

The recoiling target ions were extracted in the x-direction with a weak electric field of 6 V/cm and then traversed a field-free region twice as long as the extraction region. The recoil ions were detected with a second two-dimensional position-sensitive detector, which was set in coincidence with the projectile detector. From the position information, the recoil-ion momentum components in the y- and z-direction (defined by the initial projectile beam direction) were determined, and the x-component was obtained from the coincidence time. The ejected electron momentum was then calculated from momentum conservation as $\mathbf{p}_{el} = \mathbf{q} - \mathbf{p}_{rec}$, i.e., the data were kinematically complete. The momentum resolution for the x- and z-components was about 0.15 a.u. FWHM. In the y-direction, the resolution was significantly worse (≈ 0.35 a.u. FWHM). However, here, our interest was focused on electrons ejected into the scattering plane spanned by the initial and final projectile momenta (i.e., the xz-plane). The recoil-ion resolution in the y-direction caused some uncertainty in the definition of the scattering plane in the data analysis, but it did not affect the polar angular resolution of the electrons ejected into that plane. The resolution in the azimuthal electron angle ϕ_{el} (defining the emission plane) was about 20° FWHM. The resolution in the polar angle θ_{el} depends on θ_{el} itself and ranged from 8° to 12° .

3. Theory

The theoretical model of ionization by charged particle impact for calculating the FDCS as a function of the coherence width of the wave packet associated to the projectile was described in detail elsewhere [40,43]. Briefly, as a first step, the impact-parameter-dependent transition probability amplitude $a(\mathbf{b}, E, \Omega_e)$ was calculated ab initio, E being the energy and Ω_e the ejection angle of the electron. We numerically solved the time-dependent Schrödinger equation for the two active electrons of the target, which were moving in the combined electric field of the target core and of the projectile [13,44]. The angular part of the electronic wave function was represented in the basis of coupled symmetrized spherical harmonics [13] centered on the target, while the radial partial waves were discretized using the finite element discrete variable representation method [45]. For the time propagation of the wave function, the short iterative Lanczos method [46] with adaptive time-step size control was used.

For a given impact parameter, the transition amplitudes were extracted by projecting the time-dependent wave function onto single continuum eigenstates. We have approximated these eigenstates as a symmetrized product of single electron He^+ bound states and Coulomb continuum states. This approach was successfully applied to describe the electronic dynamics induced by negatively charged projectiles in He [13,47]; however, in the case of positively charged projectiles, it has some shortcomings due to the presence of the capture channel. The corresponding projectile bound states are poorly represented in a target-centered basis set, and they are not orthogonal to the uncorrelated single continuum eigenstates used in the calculation of the transition probability amplitudes. These two factors have an impact on the predicted transition amplitudes and thus on the predicted FDCS.

In the case of the coherent calculation, we associate a plane wave to the projectile (implying infinite transverse coherence length), and the scattering amplitude depending on the transverse momentum transfer \mathbf{q}_\perp may be obtained from an inverse Fourier transform of the probability amplitude [48].

$$R_c(\mathbf{q}_\perp, E, \Omega_e) = \frac{1}{2\pi} \int d^2\mathbf{b} e^{i\mathbf{b}\cdot\mathbf{q}_\perp} b^{2i\frac{Z_p Z_T}{v_p}} a(\mathbf{b}, E, \Omega_e) \tag{1}$$

Here, $b^{2i\frac{Z_p Z_T}{v_p}}$ is an eikonal factor accounting for the projectile–nucleus interaction, Z_p and Z_T being the charges of the two particles and v_p the velocity of the projectile.

In our model, the finite coherence width of the wave packet of the projectile is taken into account by multiplying the transition probability amplitude by a two-dimensional Gaussian.

$$R(\mathbf{q}_\perp, E, \Omega_e) = \frac{N}{2\pi} \int d^2\mathbf{b} e^{i\mathbf{b}\cdot\mathbf{q}_\perp} b^{2i\frac{Z_p Z_T}{v_p}} a(\mathbf{b}, E, \Omega_e) e^{-\frac{(b_x - b_{0x})^2}{2\sigma_x^2} - \frac{(b_y - b_{0y})^2}{2\sigma_y^2}} \tag{2}$$

Here, $\{b_x, b_y\}$ are the components of the impact parameter \mathbf{b} , while σ_x and σ_y stand for the standard deviations. x is parallel to \mathbf{q}_\perp and y is perpendicular to \mathbf{q}_\perp and to the initial trajectory of the projectile. The coherence width of the projectile in each direction is considered to be the full width at half maximum (FWHM) of the Gaussian $\Delta b_{x,y} = 2.355 \sigma_{x,y}$.

Because the center of the wave packet is considered to be on the x axis, $b_{0y} = 0$, and b_{0x} is calculated on the basis of classical scattering of the projectile off the residual He^+ ion. However, the inverse Fourier transform integrates over all impact parameters contributing to each scattering angle for a given coherence length. Therefore, only for a completely incoherent case (i.e., a coherence length of 0) does our treatment imply classical projectile trajectories. A finite coherence length, in contrast, corresponds to an uncertainty in the relation between impact parameter and scattering angle. The normalization factor N is obtained by normalizing the cross section integrated over the electron ejection angles obtained with a finite coherence width to the coherent results.

Finally, the FDCS is obtained from the scattering amplitude.

$$\frac{d^3\sigma}{dE d\Omega_e d\mathbf{q}_\perp} = p_0 |R(\mathbf{q}_\perp, E, \Omega_e)|^2 \tag{3}$$

p_0 being the projectile’s initial momentum.

4. Results and Discussion

From the kinematically complete data, we extracted FDCS for the electron ejection into the scattering plane for various fixed θ_p as a function of θ_{el} . The fixed energy loss is equivalent to an electron energy of $E_{el} = \varepsilon - I = 43.9$ eV, where I is the ionization potential of He, corresponding to an electron to projectile speed ratio of 1.04. In Figure 2, the FDCS are shown for $\theta_p = 0.1, 0.2, 0.3,$ and 0.5 mrad (as indicated in the insets). The red symbols represent data taken for the large slit distance and are reported in [36], and the blue symbols show the present data taken for a small slit distance. For simplicity, we refer to these data as coherent and incoherent, respectively. However, the data are neither completely coherent nor completely incoherent, which would require coherence lengths of infinity or zero, respectively. Here, the terms coherent and incoherent refer to the larger or smaller of the two transverse coherence lengths.

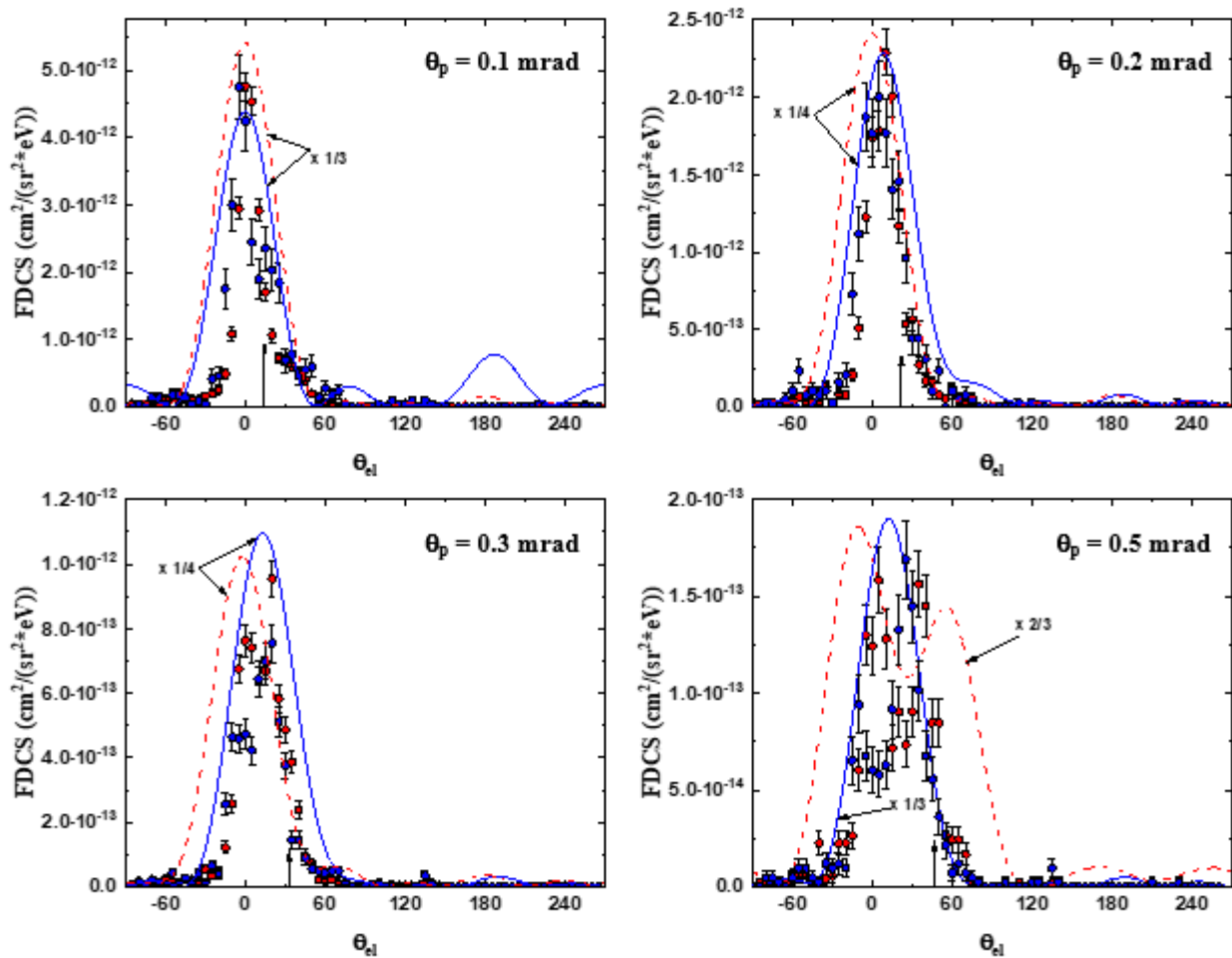


Figure 2. FDCS for electrons ejected into the scattering plane for fixed θ_p as indicated in the insets as a function of θ_{e1} . Red symbols, coherent data; blue symbols, incoherent data; red dashed curves, coherent theory; blue solid curves, incoherent theory. The vertical arrows indicate the direction of \mathbf{q} .

No measured absolute integrated cross sections have been reported yet for the incoherent case under the present kinematic conditions. Therefore, the incoherent data are normalized to the same integrated FDCS as the coherent data so that no meaningful comparison in magnitude between the two data sets is possible. At the two smaller θ_p , both the coherent and the incoherent data only exhibit a single peak structure. This is the expected behavior because the direction of \mathbf{q} is too close to $\theta_{e1} = 0$ for the binary peak to be resolvable from the forward peak, regardless of the coherence length. Here, no large differences in shape between the two data sets can be discerned, although the peak structure in the coherent case appears to be somewhat narrower. At $\theta_p = 0.3$ mrad, a separate forward/binary double-peak structure becomes visible in the coherent data. In the incoherent data, however, the minimum separating the forward and binary peaks is much shallower, if present at all, and the forward peak (relative to the binary peak) is strongly suppressed compared to the coherent data. At $\theta_p = 0.5$ mrad, the differences between the coherent and incoherent data become even larger. While in the coherent FDCS, the double-peak structure becomes even more pronounced; in the incoherent data, the forward peak is still barely separated from the binary peak and is even more suppressed compared to $\theta_p = 0.3$ mrad. This is more remarkable considering that with increasing θ_p , the direction of \mathbf{q} departs increasingly from 0° . Furthermore, the binary peak in the incoherent data is shifted in the forward direction relative to the coherent data. In summary, the data suggest that coherence effects become stronger with increasing θ_p .

The red dashed and blue solid lines in Figure 2 show our coherent and incoherent calculations. Significant discrepancies between experiment and theory are found, for both the coherent and incoherent cases. In the overall magnitude, the calculation overestimates the coherent data by as much as a factor of 4. With increasing θ_p , there are increasing discrepancies in the centroids of the maxima. Finally, the theoretical widths of the peak structures are too large, especially in the coherent case. These discrepancies could be partly due to the high sensitivity of the FDCS on the coherence length [49] combined with the uncertainty in the experimental coherence length and due to not accounting for the electron capture channel in theory. However, qualitatively, there are two important features in which theory agrees with experiment: first, at small θ_p , the differences between the coherent and incoherent calculations are relatively small, but with increasing θ_p , they become much more prominent. Second, at $\theta_p = 0.5$ mrad, the double-peak structure seen in the coherent calculation turns into a single peak in the incoherent case, located between the forward and binary peaks of the coherent FDCS, such as in the experimental data. Thus, theory provides some support for the interpretation that the double-peak structure at large θ_p for the coherent FDCS is due to interference between the first- and higher-order amplitudes. In the theoretical model, the interference emerges from a coherent superposition of different impact parameters leading to the same θ_p . In general, this does not necessarily require the presence of higher-order contributions [40,43]. However, in the present case in a pure first-order calculation, the forward peak is completely absent. Furthermore, an incoherent higher-order calculation (considering only a small interval of impact parameters) leads to only one peak. Interference between various impact parameters is therefore equivalent to interference between first- and higher-order amplitudes.

In analogy to classical optics, the coherent cross sections can be expressed as a product between the incoherent cross sections and the interference term, i.e., the ratio R between the coherent and incoherent FDCS represents the interference term. These ratios are plotted as a function of θ_{el} in Figure 3 for $\theta_p = 0.3$ and 0.5 mrad in the left and right panels, respectively. For the smaller scattering angles, the differences between the coherent and incoherent FDCS are relatively small, and the ratios mostly show statistical scatter. At $\theta_p = 0.3$ mrad, the ratios show maxima at $\theta_{el} = 0^\circ$ and 35° , which are close to the direction of \mathbf{q} indicated by the vertical arrow. The peaks are separated by a shallow minimum at about 20° . At $\theta_p = 0.5$ mrad, the peak structure at 0° and the following minimum are significantly more pronounced, where the ratio in the minimum is about a factor of 5 smaller than in the forward maximum. After the minimum, the ratios strongly rise once again, but due to the large error bars for large θ_{el} , it is not clear whether this results in a second maximum. However, the data are not inconsistent with a second maximum in the direction of \mathbf{q} at 48° . These features in the interference term extracted from the experimental data further support the interpretation that the double-peak structure observed in the coherent FDCS is due to constructive interference in the forward direction and in the direction of \mathbf{q} and destructive interference in between these directions.

Unfortunately, the theoretical ratios are dominated by the behavior in the wings of the maxima in the FDCS. As a result, the ratios are very large in regions (θ_{el} approaching -90° and 180°) where the FDCS are nearly 0, which masks the shape of the interference term in the interesting region of the double-peak structure. Therefore, a comparison between theoretical and experimental ratios does not provide any further insight.

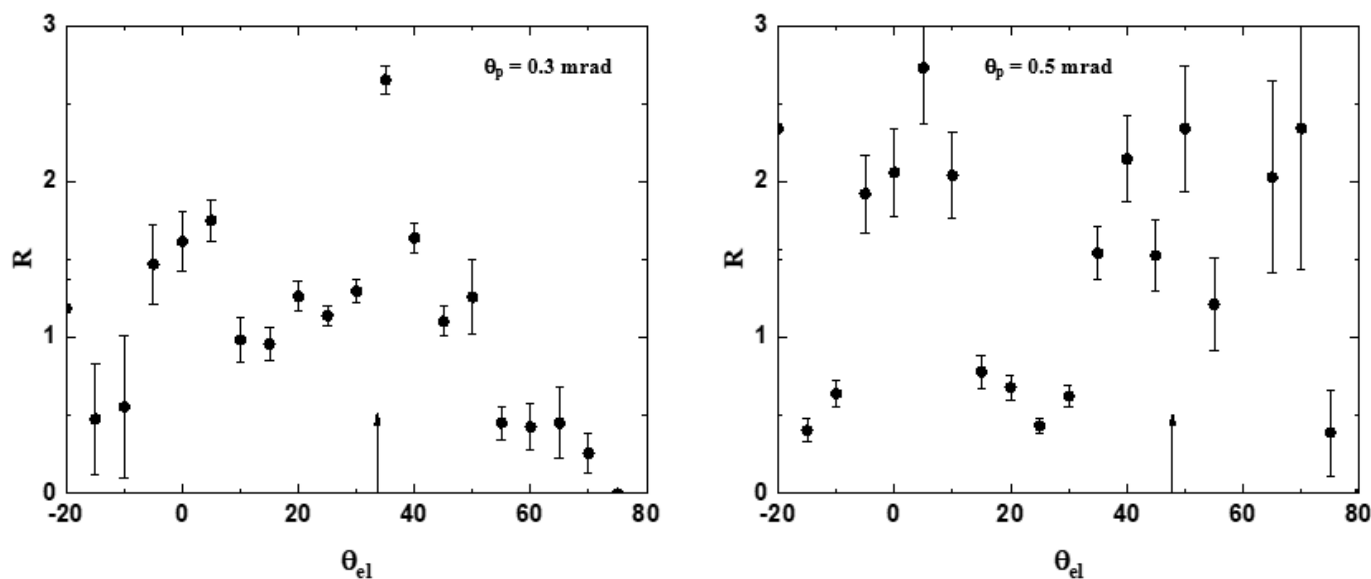


Figure 3. Ratios between the coherent and incoherent FDCS from Figure 2.

5. Conclusions and Outlook

We have measured and calculated FDCS for ionization in the velocity-matching regime for an incoherent projectile beam and compared them to data previously taken for a coherent beam. With increasing scattering angle, increasing differences between the coherent and incoherent FDCS are found. At the largest scattering angle, these differences are of qualitative nature. A double-peak structure in the coherent case is nearly turned into a single peak in the incoherent case, which is the behavior expected from a classical point of view. We therefore conclude that the double-peak structure in the coherent FDCS is likely due to constructive interference in the forward direction and in the direction of \mathbf{q} and destructive interference leading to a minimum between these directions. This conclusion is qualitatively supported by our calculations, although there are large quantitative discrepancies to the experimental data.

As an outlook, we plan to extend the experiments to other projectile energies and targets in order to investigate the interference leading to the double-peak structure more systematically. On the theoretical side, it appears important to include projectile bound states to account for the capture channel. Due to unitarity, the missing projectile states means that capture is erroneously counted as ionization in the transition amplitude. This effect is expected to have a particularly large impact in the velocity-matching regime because of the energetic proximity of the continuum electron states to the projectile bound states. Unfortunately, including projectile bound states requires a major redesign of the existing model, implying additional computational efforts and successfully concluding such a project is very time-consuming.

Author Contributions: Conceptualization, M.S.; methodology, M.S. and L.N.; software, S.B. (Sujan Bastola), A.H., L.N. and S.B. (Sandor Borbely); validation, S.B. (Sujan Bastola) and M.S.; formal analysis, S.B. (Sujan Bastola), M.D. and A.H.; investigation, all authors; data curation, S.B. (Sujan Bastola) and M.S.; writing—S.B. (Sujan Bastola); writing—review and editing, M.S.; visualization, S.B. (Sujan Bastola) and M.S.; supervision, M.S.; project administration, M.S.; funding acquisition, M.S., L.N. and S.B. (Sandor Borbely). All authors have read and agreed to the published version of the manuscript.

Funding: This research was funded by the National Science Foundation grant number PHY-2011307 and by the National Research Development and Innovation Office (NKFIH) grant no. KH 126886. S.B. was supported by the Babeş-Bolyai University under grant no. GTC 35280/18.11.2020.

Institutional Review Board Statement: Not applicable.

Informed Consent Statement: Not applicable.

Data Availability Statement: Data are available from the corresponding author.

Acknowledgments: The numerical calculations were performed using the high-performance computing resources of Babes-Bolyai University.

Conflicts of Interest: The authors declare no conflict of interest.

References

1. Rescigno, T.N.; Baertschy, M.; Isaacs, W.A.; McCurdy, C.W. Collisional breakup in a quantum system of three charged particles. *Science* **1999**, *286*, 2474. [[CrossRef](#)] [[PubMed](#)]
2. Schulz, M.; Moshhammer, R.; Fischer, D.; Kollmus, H.; Madison, D.H.; Jones, S.; Ullrich, J. Three-Dimensional Imaging of Atomic Four-Body Processes. *Nature* **2003**, *422*, 48. [[CrossRef](#)] [[PubMed](#)]
3. Brauner, M.; Briggs, J.S.; Klar, H. Triply-differential cross sections for ionisation of hydrogen atoms by electrons and positrons. *Phys. B* **1989**, *22*, 2265. [[CrossRef](#)]
4. Ciappina, M.F.; Cravero, W.R.; Garibotti, C.R. Influence of the electron binding energy in the distortion of the initial state in ion-atom collisions. *Phys. Rev. A* **2004**, *70*, 062713. [[CrossRef](#)]
5. Foster, M.; Peacher, J.L.; Schulz, M.; Madison, D.H.; Chen, Z.; Walters, H.R.J. Unexpected Higher-Order Effects in Charged Particle Impact Ionization at High Energies. *Phys. Rev. Lett.* **2006**, *97*, 093202. [[CrossRef](#)]
6. Cappello, C.D.; Rezkallah, Z.; Houamer, S.; Charpentier, I.; Hervieux, P.A.; Ruiz-Lopez, M.F.; Dey, R.; Roy, A.C. Second-order Born approximation for the ionization of molecules by electron and positron impact. *Phys. Rev. A* **2011**, *84*, 032711. [[CrossRef](#)]
7. Kouzakov, K.A.; Zaytsev, S.A.; Popov, Y.V.; Takahashi, M. Singly ionizing 100-MeV/amu C⁶⁺+He collisions with small momentum transfer. *Phys. Rev. A* **2012**, *86*, 032710. [[CrossRef](#)]
8. Czipa, L.; Nagy, L. Two-center interference in the ionization of H₂ by ion impact: Comparison of different models. *Phys. Rev. A* **2017**, *95*, 062709. [[CrossRef](#)]
9. Voitkiv, A.B. Single ionization of helium by 1-MeV protons. *Phys. Rev. A* **2017**, *95*, 032708. [[CrossRef](#)]
10. Gulyás, L.; Egri, S.; Igarashi, A. Theoretical investigation of the fully differential cross sections for single ionization of He in collisions with 75-keV protons. *Phys. Rev. A* **2019**, *99*, 032704. [[CrossRef](#)]
11. Ciappina, M.F.; Pindzola, M.S.; Colgan, J. Fully differential cross section for O⁸⁺-impact ionization of Li. *Phys. Rev. A* **2013**, *87*, 042706. [[CrossRef](#)]
12. Walters, H.R.J.; Whelan, C.T. Differential ionization of Li(2s) and Li(2p) under proton and O⁸⁺ impact. *Phys. Rev. A* **2014**, *89*, 032709. [[CrossRef](#)]
13. Borbély, S.; Feist, J.; Tókési, K.; Nagele, S.; Nagy, L.; Burgdörfer, J. Ionization of helium by slow antiproton impact: Total and differential cross sections. *Phys. Rev. A* **2014**, *90*, 052706. [[CrossRef](#)]
14. Baxter, M.; Kirchner, T.; Engel, E. Time-dependent spin-density-functional-theory description of He⁺-He collisions. *Phys. Rev. A* **2017**, *96*, 032708. [[CrossRef](#)]
15. Abdurakhmanov, I.B.; Bailey, J.J.; Kadyrov, A.S.; Bray, I. Wave-packet continuum-discretization approach to ion-atom collisions including rearrangement: Application to differential ionization in proton-hydrogen scattering. *Phys. Rev. A* **2018**, *97*, 032707. [[CrossRef](#)]
16. Crooks, G.B.; Rudd, M.E. Experimental Evidence for the Mechanism of Charge Transfer into Continuum States. *Phys. Rev. Lett.* **1970**, *25*, 1599. [[CrossRef](#)]
17. Sarkadi, L.; Palinkas, J.; Köver, A.; Berenyi, D.; Vajnai, T. Observation of Electron Capture into Continuum States of Neutral Atoms. *Phys. Rev. Lett.* **1989**, *62*, 527. [[CrossRef](#)]
18. Vajnai, T.; Gaus, A.D.; Brand, J.A.; Htwe, W.; Madison, D.H.; Olson, R.E.; Peacher, J.L.; Schulz, M. Observation of Postcollision Effects in the Scattered Projectile Spectra for Ionizing Proton-Helium Collisions. *Phys. Rev. Lett.* **1995**, *74*, 3588. [[CrossRef](#)]
19. Tribedi, L.C.; Richard, P.; Dehaven, W.; Gulyás, L.; Gealy, M.W.; Rudd, M.E. Ionization dynamics in fast ion-atom collisions. I. Energy and angular distributions of low-energy electrons emitted in ionization of He by bare carbon ions. *Phys. Rev. A* **1998**, *58*, 3619. [[CrossRef](#)]
20. Weber, T.; Khayyat, K.; Dörner, R.; Rodríguez, V.D.; Mergel, V.; Jagutzki, O.; Schmidt, L.; Müller, K.A.; Afaneh, F.; Gonzalez, A.; et al. Abrupt Rise of the Longitudinal Recoil Ion Momentum Distribution for Ionizing Collisions. *Phys. Rev. Lett.* **2001**, *86*, 224. [[CrossRef](#)]
21. Sarkadi, L.; Gulyas, L.; Lugosi, L. Postcollision interaction and two-center effects in ionizing collisions. *Phys. Rev. A* **2002**, *65*, 052715. [[CrossRef](#)]
22. Schulz, M.; Laforge, A.C.; Egodapitiya, K.N.; Alexander, J.S.; Hasan, A.; Ciappina, M.F.; Roy, A.C.; Dey, R.; Samolov, A.; Godunov, A.L. Doubly differential spectra of scattered protons in ionization of atomic hydrogen. *Phys. Rev. A* **2010**, *81*, 052705. [[CrossRef](#)]
23. Chowdhury, U.; Schulz, M.; Madison, D.H. Differential cross sections for single ionization of H₂ by 75-keV proton impact. *Phys. Rev. A* **2011**, *83*, 032712. [[CrossRef](#)]

24. Walters, H.R.J.; Whelan, C.T. Differential ionization of a one-electron target under bare-ion impact: Application to proton-impact ionization of atomic hydrogen. *Phys Rev. A* **2015**, *92*, 062712. [[CrossRef](#)]
25. Silvus, A.; Dhital, M.; Bastola, S.; Buxton, J.; Klok, Z.; Ali, E.; Ciappina, M.F.; Boggs, B.; Cikota, D.; Madison, D.H.; et al. Target dependence of post-collision effects in ionization by proton impact. *J. Phys. B* **2019**, *52*, 125202. [[CrossRef](#)]
26. Ullrich, J.; Moshhammer, R.; Dorn, A.; Dörner, R.; Schmidt, L.; Schmidt-Böcking, H. Recoil-ion and electron momentum spectroscopy: Reaction-microscopes. *Rep. Prog. Phys.* **2003**, *66*, 1463. [[CrossRef](#)]
27. Dörner, R.; Mergel, V.; Jagutzki, O.; Spielberger, L.; Ullrich, J.; Moshhammer, R.; Schmidt-Böcking, H. Cold Target Recoil Ion Momentum Spectroscopy: A 'momentum microscope' to view atomic collision dynamics. *Phys. Rep.* **2000**, *330*, 95. [[CrossRef](#)]
28. Schulz, M.; Madison, D.H. Studies of the Few-Body Problem in Atomic Break-Up Processes. *Intern. J. Mod. Phys. A* **2006**, *21*, 3649. [[CrossRef](#)]
29. Gassert, H.; Chuluunbaatar, O.; Waitz, M.; Trinter, F.; Kim, H.-K.; Bauer, T.; Laucke, A.; Müller, C.; Voigtsberger, J.; Weller, M.; et al. Agreement of Experiment and Theory on the Single Ionization of Helium by Fast Proton Impact. *Phys. Rev. Lett.* **2016**, *116*, 073201. [[CrossRef](#)]
30. Maydanyuk, N.V.; Hasan, A.; Foster, M.; Tooke, B.; Nanni, E.; Madison, D.H.; Schulz, M. Projectile-Residual-Target-Ion Scattering after Single Ionization of Helium by Slow Proton Impact. *Phys. Rev. Lett.* **2005**, *94*, 243201. [[CrossRef](#)]
31. Schulz, M.; Hasan, A.; Maydanyuk, N.V.; Foster, M.; Tooke, B.; Madison, D.H. Kinematically complete experiment on single ionization in 75-keV p+He collisions. *Phys. Rev. A* **2006**, *73*, 062704. [[CrossRef](#)]
32. Hasan, A.; Sharma, S.; Arthanayaka, T.P.; Lamichhane, B.R.; Remolina, J.; Akula, S.; Madison, D.H.; Schulz, M. Triple differential study of ionization of H₂ by proton impact for varying electron ejection geometries. *J. Phys. B* **2014**, *47*, 215201. [[CrossRef](#)]
33. Schulz, M.; Moshhammer, R.; Perumal, A.N.; Ullrich, J. Triply differential single-ionization cross sections in fast ion-atom collisions at large perturbation. *J. Phys. B* **2002**, *35*, L161. [[CrossRef](#)]
34. Schulz, M.; Najjari, B.; Voitkiv, A.B.; Schneider, K.; Wang, X.; Laforge, A.C.; Hubele, R.; Goullon, J.; Ferreira, N.; Kelkar, A.; et al. Postcollision effects in target ionization by ion impact at large momentum transfer. *Phys. Rev. A* **2013**, *88*, 022704. [[CrossRef](#)]
35. Dhital, M.; Bastola, S.; Silvus, A.; Hasan, A.; Lamichhane, B.R.; Ali, E.; Ciappina, M.F.; Lomsadze, R.A.; Cikota, D.; Boggs, B.; et al. Few-body dynamics underlying postcollision effects in the ionization of H₂ by 75-keV proton impact. *Phys. Rev. A* **2019**, *99*, 062710. [[CrossRef](#)]
36. Dhital, M.; Bastola, S.; Silvus, A.; Lamichhane, B.R.; Ali, E.; Ciappina, M.F.; Lomsadze, R.; Hasan, A.; Madison, D.H.; Schulz, M. Target dependence of postcollision interaction effects on fully differential ionization cross sections. *Phys. Rev. A* **2019**, *100*, 032707. [[CrossRef](#)]
37. Egodapitiya, K.N.; Sharma, S.; Hasan, A.; Laforge, A.C.; Madison, D.H.; Moshhammer, R.; Schulz, M. Manipulating Atomic Fragmentation Processes by Controlling the Projectile Coherence. *Phys. Rev. Lett.* **2011**, *106*, 153202. [[CrossRef](#)] [[PubMed](#)]
38. Schulz, M. The Role of Projectile Coherence in the Few-Body Dynamics of Simple Atomic Systems. In *Advances in Atomic, Molecular, and Optical Physics*; Arimondo, E., Lin, C.C., Yelin, S., Eds.; Elsevier: Amsterdam, The Netherlands, 2017; Volume 66, pp. 508–543.
39. Barrachina, R.O.; Navarrete, F.; Ciappina, M.F. Quantum coherence enfeebled by classical uncertainties. *Phys. Rev. Res.* **2020**, *2*, 043353. [[CrossRef](#)]
40. Nagy, L.; Jarai-Szabo, F.; Borbely, S. The effect of projectile wave packet width on the fully differential ionization cross-sections. *J. Phys. B* **2018**, *51*, 144005. [[CrossRef](#)]
41. Sarkadi, L.; Fabre, I.; Navarrete, F.; Barrachina, R.O. Loss of wave-packet coherence in ion-atom collisions. *Phys. Rev. A* **2016**, *93*, 032702. [[CrossRef](#)]
42. Gaus, A.D.; Htwe, W.; Brand, J.A.; Gay, T.J.; Schulz, M. Energy-Spread Measurements of Various Ion Sources. *Rev. Sci. Instrum.* **1994**, *65*, 3739. [[CrossRef](#)]
43. Nagy, L.; Jarai-Szabo, F.; Borbely, S.; Arthanayaka, T.; Lamichhane, B.R.; Hasan, A.; Schulz, M. *The State-of-the-Art-Reviews on Energetic Ion-Atom and Ion-Molecule Collisions*; Belkic, D., Bray, I., Kadyrov, A., Eds.; World Scientific Publishing: Singapore, 2019; Volume 2, p. 129.
44. Feist, J.; Nagele, S.; Pazourek, R.; Persson, E.; Schneider, B.I.; Collins, L.A.; Burgdörfer, J. Nonsequential two-photon double ionization of helium. *Phys. Rev. A* **2008**, *77*, 043420. [[CrossRef](#)]
45. Rescigno, T.N.; McCurdy, C.W. Numerical grid methods for quantum-mechanical scattering problems. *Phys. Rev. A* **2000**, *62*, 032706. [[CrossRef](#)]
46. Park, T.J.; Light, J.C. Unitary quantum time evolution by iterative Lanczos reduction. *J. Chem. Phys.* **1986**, *85*, 5870. [[CrossRef](#)]
47. Borbély, S.; Tong, X.-M.; Nagele, S.; Feist, J.; Březinová, I.; Lackner, F.; Nagy, L.; Tőkési, K.; Burgdörfer, J. Electron correlations in the antiproton energy-loss distribution in He. *Phys. Rev. A* **2018**, *98*, 012707. [[CrossRef](#)]
48. Rivarola, R.; Fainstein, P. Electron emission in collisions of highly charged ions with atoms and diatomic molecules. *Nucl. Instrum. Meth. Phys. Res. B* **2003**, *205*, 448.
49. Arthanayaka, T.; Lamichhane, B.R.; Hasan, A.; Gurung, S.; Remolina, J.; Borbély, S.; Járjai-Szabó, F.; Nagy, L.; Schulz, M. Fully Differential Study of Wave Packet Scattering in Ionization of Helium by Proton Impact. *J. Phys. B* **2016**, *49*, 13LT02. [[CrossRef](#)]